# Integrated Slow-Light Enhanced Silicon Photonic Modulators for RF Photonic Links

Stephen R. Anderson, Amir Begović, and Z. Rena Huang, *Member, IEEE*

***Abstract*—An integrated RF-photonic link that consists of a slow-light enhanced silicon (Si) electro-optic modulator, a single mode Si optical waveguide and a silicon-germanium (SiGe) photodetector was fabricated using a Si photonic standard foundry service. The third-order intermodulation distortion (IMD3) of the RF signals and the link spur-free dynamic range (SFDR) were characterized through a two-tone test method. The Si Mach-Zehnder modulator architecture is designed to have unequal arms to operate on a simplified driving scheme. As a result, on-chip thermal heaters can be omitted, and the modulator can configure near its quadrature point by adjusting the wavelength to the modulator. Owning to enhanced light-matter interaction in the slow-light region, an increased slope efficiency is observed in the modulator. By selecting the optimal DC bias to the grating and the reference arms of the modulator, a SFDR of 96 dB/Hz$^{2/3}$ can be obtained in the RF link at the slow light region. The slow-light modulator also displays increased modulation efficiency, allowing for a reduced footprint for large array integration.**

***Index Terms*—Grating, modulator, photonics, RF-photonics, slow-light.**

## I. Introduction

THE photonic modulator is a critical component in a myriad of radio-frequency (RF) photonic systems, serving to transduce RF signals into the optical domain. $LiNbO_3$ modulators represent the current industry preference, as it has low insertion loss and allows for RF links to operate at high speed while maintaining a large link spur-free dynamic range (SFDR). An integrated chip-scale RF photonic link offers significant size, weight, power, and cost (SWaP-C) advantages and are in high demand for many applications. In recent years, efforts to heterogeneously integrate thin-film $LiNbO_3$ onto a silicon (Si) platform have demonstrated some promise [1], [2] but have not been widely adopted by silicon photonics foundries due to the relative difficulty in processing. The Si optical modulator is an attractive alternative technology, and has been studied extensively for both high-speed optical interconnection applications [3], [4] and analog RF photonic applications [5] in the last two decades.

Recently, Si Mach-Zehnder modulators (MZM) realized with foundry processes have been demonstrated for RF photonic links [6]–[8]. However, there are several practical concerns not sufficiently addressed so far. First, many current MZM designs have incorporated silicon heaters [9] in both MZM arms that are addressed separately to unbalance the phase shifter to set the MZM at its quadrature point. The on-chip heaters not only add extra chip surface area but also require stringent thermal isolation. Second, Si MZMs typically have millimeters-long phase shifters, and they require differential-driving [10], [11] or distributed-driving [12] techniques which increases the system complexity.

In this work, we introduce a novel Si MZM design that utilizes Bragg grating based slow-light MZM (SLM) that was also fabricated in a standard Si foundry for potential adoption in real world applications. First, the SLM has enhanced field-matter interaction leading to an increased modulation efficiency. Due to this increased efficiency, this design offers a solution with a reduced footprint for densely-integrated RF-optical systems constrained by chip surface area, such as when RF modulators are used in an arrayed RF link application [13], [14]. Second, a smaller MZM would potentially enable a simpler driving scheme. The SLM of this work is placed in an unequal phase shifter architecture so that the heaters can be omitted, relying on wavelength setting and/or adjusting the DC bias voltages to set the modulator near its quadrature point. Si Bragg grating operation stability was analyzed in a prior study in our group and reported a band-edge shift due to temperature sensitivity up to 70\,pm/°C [15].

Slow-light architectures, such as photonic crystal modulators and Bragg-like gratings, have been previously examined in terms of achievable electro-optic bandwidth, and digital parameters such as bit-error-rate [16]–[18]. In this work, it is the first time that modulator analog performance parameters, including SFDR and third-order intermodulation distortion (IMD3) are evaluated for a Bragg grating slow-light modulator.

## II. Modulator Design and Theory

### 1. Device Structure

The integrated RF link, including the SLM, waveguides and a silicon-germanium (SiGe) photodetector (PD), was fabricated using the American Institute of Manufacturing Photonics (AIM Photonics) multi-project wafer (MPW) process on a Si-on-insulator (SOI) substrate that has 220 nm of Si layer on top of a buried oxide of 3 $\mu$m thick. A schematic of the SLM structure is depicted in Fig. 1(a). The input optical signal is split into two paths by a y-splitter and recombined afterward by

Manuscript received 13 May 2022; revised 10 June 2022; accepted 17 June 2022. Date of publication 23 June 2022; date of current version 24 August 2022. This work was supported in part by ARL under Grant W911NF-16-2-0049. *(Corresponding author: Z. Rena Huang.)*

The authors are with the Electrical, Computer and Systems Engineering Department, Rensselaer Polytechnic Institute, Troy, NY 12180-3522 USA (e-mail: anders8@rpi.edu; begova@rpi.edu; huangz3@rpi.edu).

Digital Object Identifier 10.1109/JPHOT.2022.3185888

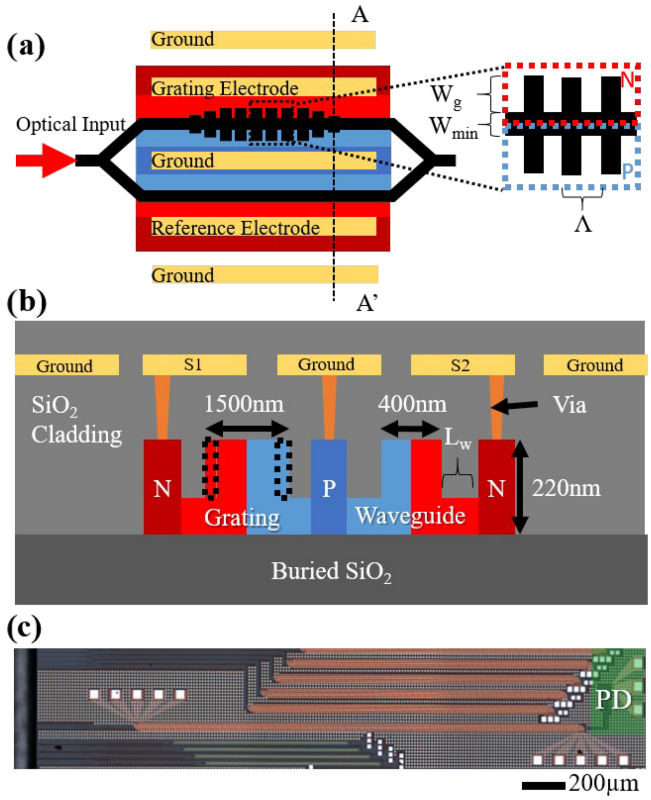


Fig. 1. (a) Schematic of the slow-light enhanced modulator. The detail view labels the geometric parameters of the grating, center waveguide width $W_{min}$, grating bar width $W_g$, and period $\Lambda$. (b) Slow-light enhanced modulator cross-section A-A'. (Not drawn to scale) A signal S1 is applied to the grating electrode, while a signal S2 is applied to the reference electrode. In the single-driven scheme, S1 includes a junction bias and a small-signal RF component. S2 contains only a DC bias component. The biasing conditions on the grating and reference electrodes are detailed in Section III. (c) Optical micrograph of the 2 mm slow light enhanced Si MZM. The SLM is connected to an on-chip SiGe PD with a Si nanowire waveguide on the same die.

a y-combiner following the design in [19]. A 2 mm long Bragg grating waveguide is incorporated in one path of the MZM, referred to as the grating arm, while the other path contains a straight waveguide and is referred to as the reference arm. The grating has a period $\Lambda = 282$ nm. The center waveguide has a width of $W_{min} = 400$ nm to guide the optical field and the grating bar width $W_g$ follows a super-Gaussian apodization profile [20] with a maximum $W_g$ of 550 nm. The apodization serves to suppress the side band oscillations and reduce mode mismatch between the straight waveguide and the slow-light grating waveguide.

A cross section of the modulator is shown in Fig. 1(b). The waveguide slab has a thickness of 110 nm, and it extends for a distance of $L_w = 3$ $\mu$m to connect to the tungsten via. A PN junction is formed in the center of the waveguide, with moderate doping concentrations on the order of $1\times10^{18}$ cm$^{-3}$. A separation of 10 nm is set in the layout between the P and N regions. The travelling wave electrodes are terminated with a DC-block and a 50 Ω resistor. To improve signal isolation, two additional ground lines surrounding the metal traces are designed.

A standard AIM SiGe PD with a responsivity of 0.9 A/W (at $\lambda = 1550$ nm) was used to convert the light to electrical signals. Both the SLM and SiGe PD lie within the MPW die and are interconnected by an embedded single-mode silicon photonic waveguide.

### 2. *Nonlinearities in Si MZM*

The linearity of a modulator informs which analog applications it may be suited for. In particular, the input third-order intercept point (IIP3) is often used as a specification of nonlinearity for RF-devices, while SFDR may be used to characterize the overall linear performance of an RF (or RF-Photonic) link. The output intensity of the SLM, $I_{op}$, depends on the complex amplitude and phase imparted by each arm. The generalized transfer function of a MZI may be described as

$$I_{op} = \frac{1}{4}\left|e^{-\alpha_1 L_1}e^{-j\beta_1 L_1} + e^{-\alpha_2 L_2}e^{-j\beta_2 L_2}\right|^2, \quad (1)$$

where $\alpha$ is the loss per unit length, and $\beta$ is the propagation constant, defined as $\beta = \frac{2\pi n_{eff}}{\lambda}$ and $n_{eff}$ is the effective index. Subscripts "1" and "2" denote either arm of an MZM. Both $\alpha$ and $\beta$ are functions of the operating wavelength. Unequal loss in the optical paths will result in deteriorated extinction ratio. For an ideal, lossless modulator with equal phase shifter length, Eq. (1) reduces to a squared cosine

$$\lim_{\alpha\to 0} I_{op} \approx \cos^2\left(\left(\beta_2 - \beta_1\right)L\right) = \cos^2\left(\varphi + \Delta\varphi\right), \quad (2)$$

where $\varphi$ is the phase difference between the two arms under DC condition while $\Delta\varphi$ is the additional phase variation caused by the input RF signal, $\tilde{V}_{RF}$. The MZM responds to the input $\tilde{V}_{RF}$ most linearly when the DC phase component $\varphi$ is selected such that the MZM operates near its quadrature. Theoretically, if $\Delta\varphi(\tilde{V}_{RF})$ could follow an inverse-cosine dependence for an ideal MZM, the composite transfer function is linear. For a practical MZM device, the nonlinear RF signal distortions come from multiple sources.

The square root dependence of depletion layer width on the driving voltage counts for a primary source of the signal distortion. Application of a small signal $\tilde{v}_{RF}$ varies with the depletion width, w, according to

$$w\left(\tilde{v}_{RF}\right) \approx \sqrt{\frac{2\varepsilon_{Si}}{q}\frac{\left(N_A + N_D\right)}{\left(N_A N_D\right)}\left(V_{bi} - V_{DC} - \tilde{v}_{RF}\right)} \quad (3)$$

where q is the electron charge, $\varepsilon_{Si}$ is the permittivity of silicon, $N_A$ ($N_D$) is the acceptor (donor) concentration, $V_{bi}$ is the junction built-in voltage, and $V_{DC}$ is the applied DC bias voltage across the junction. The carrier density modulation within the depletion layer $w\ (\tilde{v}_{RF})$ leads to the change of the refractive index, $\Delta n$ and the absorption coefficient $\Delta\alpha$ following a linear relation [21]:

$$\Delta n \propto -\left(\frac{\Delta N_{e,h}}{\sqrt{\varepsilon_{Si}}}\right) \text{ and } \Delta\alpha \propto \left(\frac{\Delta N_{e,h}}{\sqrt{\varepsilon_{Si}}}\right), \quad (4)$$

where $\Delta N_{e,h}$ is the change in electron or hole concentration. The effective index of the Si waveguide also follows a nonlinear relation with the weighted spatial integral of the optical mode

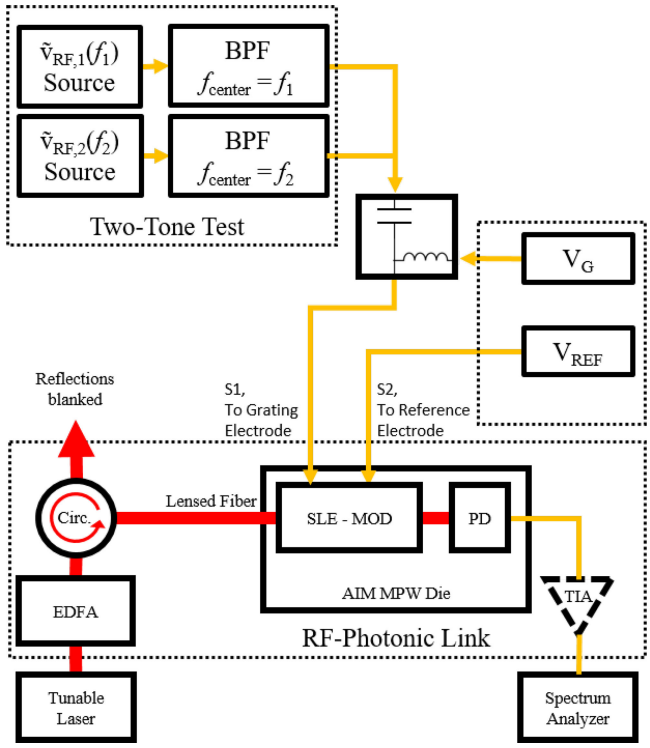


Fig. 2. A schematic of the two-tone test experimental setup. Fundamental and resulting IMD3 tones are measured at the output spectrum analyzer. BPF – Band-pass filter, SLE-MOD – slow-light enhanced modulator, TIA – low-noise trans-impedance amplifier, Circ. – Optical Circulator. The biasing circuit for the PD is not shown. $\boldsymbol{S_1} = \tilde{v}_{\boldsymbol{RF},1}(500\ \boldsymbol{MHz}) + \tilde{v}_{\boldsymbol{RF},2}(515\ \boldsymbol{MHz}) + \boldsymbol{V_G}$ and $\boldsymbol{S_2} = \boldsymbol{V_{REF}}$ .

with the free carrier plasma density. The varying group index due to apodization near the photonic band edge of the grating is another source of nonlinearity. Kerr effect of Si material induces additional nonlinear optical distortion. The measured RF link linearity combines all sources of signal distortion, where each source of nonlinearity may contribute to, or partially cancel, the total distortion [7].

## III. Experimental Characterization

The two-tone test was utilized to characterize the nonlinearity and SFDR of the SLM. The experimental setup is depicted in Fig. 2. The modulator die is mounted on an external thermo-electric cooler at a fixed temperature of 20°C. A polarization-maintaining lensed fiber injects light onto the die from a wavelength tunable laser (Agilent 81682A). An Erbium-doped fiber amplifier (EDFA) was connected after the laser to produce an optical power up to 20 dBm. The fiber to chip coupling loss is estimated to be $\sim$ 2 dB/facet. At the output of the RF-photonic link, the PD output is optionally amplified by an external low-noise amplifier (MiniCircuits ZHL-2010+) and is collected by an RF spectrum analyzer (Advantest R3271). Under testing, DC biases are applied to the grating arm and the reference arm, denoted as $V_G$ and $V_{REF}$, respectively.

A dual-channel microwave generator (WindFreak SynthHD Pro) supplies the RF signals at frequencies $f_1$ = 500 MHz and $f_2$ = 515 MHz with equal amplitude. For a prototype demonstration, frequencies around either 500 MHz or 1 GHz are often used [7], [ 11], [27]. These tones, combined with the grating arm DC bias $V_G$ by a bias-tee, are applied to the grating electrode. The DC bias voltage $V_{REF}$ varies to obtain different MZM operation condition. Band-pass filters tuned to the center frequency of each source to provide signal isolation as well as rejecting reflected RF signals by >40 dB. Separately, an optical circulator is used to prevent feedback from the chip reflecting into the input laser source and EDFA.

The SLM and other components in the RF link will cause spurious power at harmonics of the input frequencies as well as intermodulation products: $f_1 \pm f_2$, $f_1 \pm 2f_2$, $2f_1 \pm f_2$, *etc.* In a typical application where the input tones are closely spaced, the third-order intermodulation distortion products (IMD3) are within the same band as the input tones, making them difficult to filter, so IMD3 suppression is the main concern in this work. The equal input tone powers are systematically increased, and the fundamental power and IMD3 power are monitored at the spectrum analyzer. We will seek an operating point of the SLM that minimizes the IMD3 spur of the RF link.

## IV. Results and Discussion

In a RF link, the modulator, the Si waveguide, the on-chip SiGe PD and the external amplifier all contribute to the RF signal distortion. SFDR is a measure of link linearity, and the modulator performance must be analyzed in the context of the entire RF link. The best-case insertion loss of the modulator and photodetector on-chip is −13.5 dB, which includes approximately 2 dB loss from the lensed-fiber/chip interface. Low-noise trans-impedance amplifiers (TIAs) are typically included in two-tone measurement. For this work we have omitted the TIA, since the PD output power is sufficiently high. The measurements are limited by the noise floor of the spectrum analyzer at -110 dBm with 10 kHz bandwidth.

### A. Slow Light Enhancement of MZM DC Response

We first characterized the transmission spectrum of a slow-light grating waveguide fabricated on the same AIM die as the SLM. Using a tunable laser ($\lambda$ = 1460 nm to 1580 nm), we observed two photonic bandgaps. In this work, the apodization is designed to suppress the side bands of the right side of the lowest order band edge [23] so the SLM testing focuses on the wavelength range of 1545-1555 nm.

The transmission spectra of the MZM output are depicted in Fig. 3(a). The slow-light effect can be seen by the narrowing of the free spectrum range (FSR) in the MZM transmission when approaching the band-edge. The detail of Bragg grating design was reported in a prior work [20]. The group index ($n_g$) of the Bragg grating waveguide was characterized using an interferometric method [20], [24]. The measured $n_g$ decreases monotonically from the band edge at $\lambda = 1545$ nm to $\sim$ 1548 nm from a maximum $n_g = 11$ to 4.5. At $\lambda = 1550$ nm, the slow light effect is much weaker and can be considered negligible. The modulation efficiency of the SLM was tested at $\lambda = 1545.15$ nm and $\lambda = 1554.51$ nm for comparison, as shown in Fig. 3(b). At

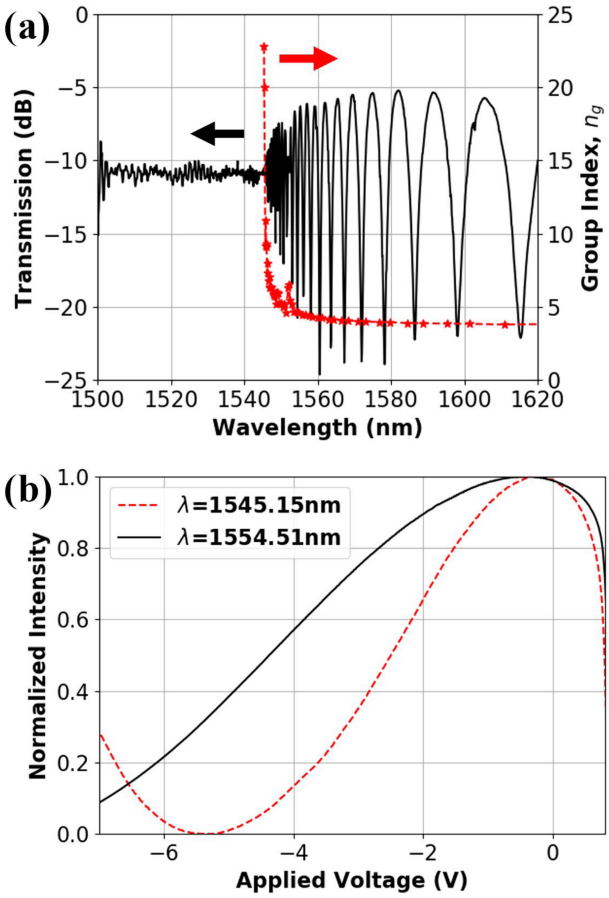


Fig. 3. (a) The transmission spectrum of the unbalanced MZM under 0V applied bias, and the measured group index of the Bragg grating waveguide. The FSR of adjacent peaks is proportional to the slow light effect. The power transmission of the Bragg grating waveguide is proportional to the interference pattern intensity, i.e., following the envelope of the MZM fringes. (b) Normalized intensity as a function of applied voltage, VG. For each case, VREF = 0 V. The two operating wavelengths are chosen to represent the modulation near and far from the band edge. For each case, the bias corresponding to the maximum transmission is approximately equal. Near to the band edge, the resulting $V\pi$ = 5.095 V ($V\pi \cdot L$ = 1.019 V·cm), whereas far from the band edge a $\pi$-phase shift is not achieved until the modulator is driven into the breakdown regime.

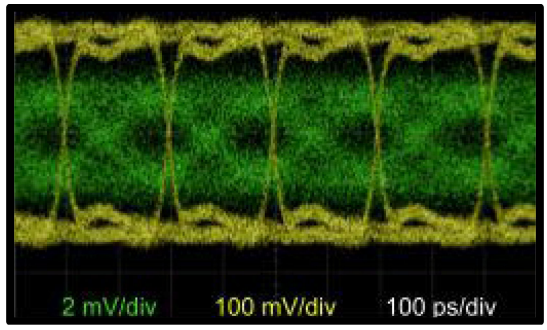


Fig. 4. An example eye diagram for the SLM. The eye diagram test is conducted at a wavelength of 1550 nm, 500 mVpp, -1.75 V DC, and at a speed of 5 Gbps. A PRBS7 signal is used and shown in yellow, while the modulator output is plotted in green.

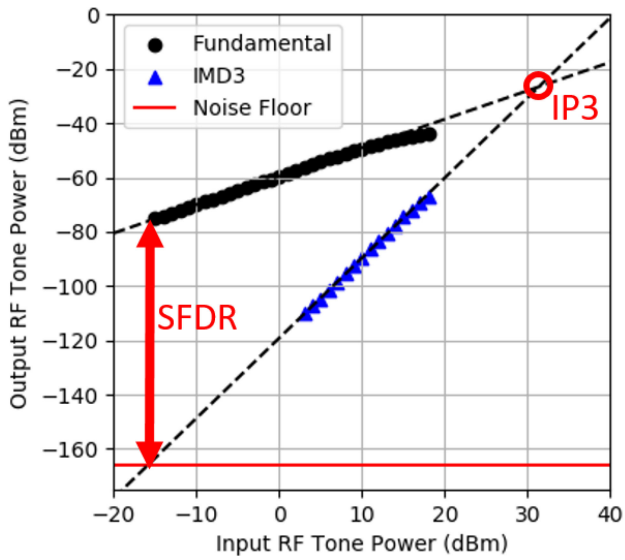


Fig. 5. A representative plot of SFDR when $V_G = V_{REF}$ = -3 V, at the slow light wavelength 1545.15 nm. The SFDR is defined as the distance between the 1Hz bandwidth noise floor and the fundamental tone where the IMD3 tone power equals the noise floor. Similarly, the IP3 figure-of-merit is defined by extrapolation to the point where the fundamental and IMD3 tone powers would be equal, if no compression occurred at high input tone powers. Dashed lines are constructed lines extrapolating the measured data.

the reverse bias -5.33 V, the SLM reaches its minimum output at $\lambda$ = 1545.15 nm while the SLM needs to bias at a much higher voltage to the avalanche breakdown region to reach its minimum when $\lambda$ = 1554.51 nm. The tested figure-of-merit $V_\pi \cdot L$ is ~1 V·cm in the slow light regime under depletion operation.

### *B. SLM Bandwidth Characterization*

The intrinsic bandwidth of depletion type Si modulators is ~50 GHz [25]. However, both the traveling wave electrode design and the driving circuit impact the RF bandwidth of the modulator. Additionally, the insertion loss of the modulator will also indirectly impact the bandwidth as a lossy optical link results in reduced sensitivity in the PD. For an RF link, the loss figure or link gain can be evaluated from the slope efficiency, which will be reported in Section IV D.

The digital application of the SLM is not the focus of this work, but we measured the eye diagram performance of the SLM. Measurements were performed with an input laser at a $\lambda$ = 1550 nm. There is a tradeoff between stronger slow-light and the resulting output power. A sufficiently high output power is required to make a decent eye-diagram. The modulation signal is a 7-bit pseudo-random bit sequence (PRBS7), applied to the SLM using an arbitrary waveform generator (AWG). The SLM works up to a speed of 8 Gbps and an example measurement taken at a speed of 5 Gbps is shown in Fig. 4.

### *C. SFDR Optimization for Bias Point Selection*

The link SFDR is sensitive to a wide range of parameters of the SLM, including the selected operating wavelength and DC bias voltages on the phase shifter and the reference arm. A representative plot of SFDR computation is provided in Fig. 5, representing the dynamic range of the fundamental tone before

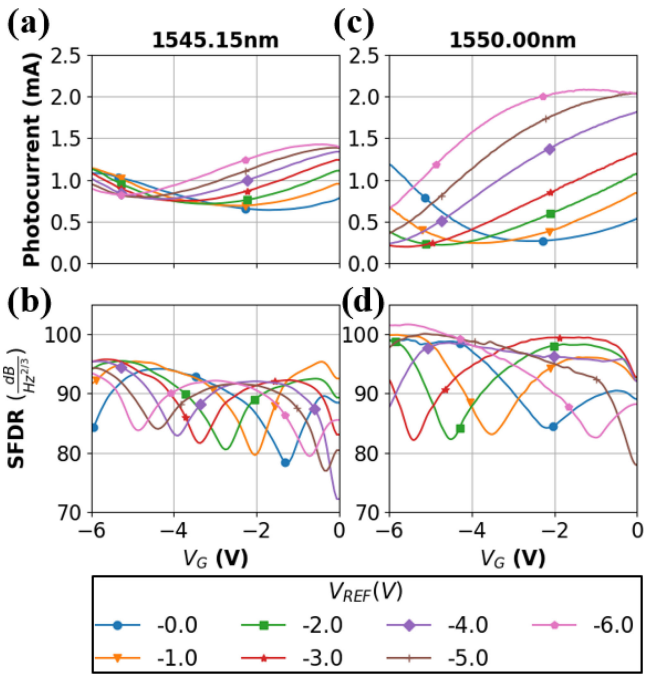


Fig. 6. Photocurrent and SFDR as a function of grating arm bias $V_G$ and reference arm bias $V_{REF}$ at selected wavelengths. a,b) at slow-light wavelength 1545.15 nm, c,d) at 1550.00 nm far from the band-edge.

the IMD3 tone "spur" is greater than the noise floor. The SFDR is reported with reference to a 1 Hz bandwidth. For $V_G = V_{REF} =$ -3V at a slow light wavelength 1545.15 nm, the SFDR is 90.86 dB/Hz$^{2/3}$. The IIP3 occurs at +31.4 dBm, and the 1 dB compression point occurs at +12.5 dBm. Subsequent measurements of SFDR in this work were measured from a single input tone power below the 1 dB compression point.

Next, the bias voltages $V_G$ and $V_{REF}$ are swept at selected wavelengths, to determine the optimal biasing point for linear operation. At a fixed $V_{REF}$ and a slow-light condition, the quadrature point of the SLM is set by varying $V_G$, as shown in Fig. 6. For example, with $V_G$ fixed at -3 V and $\lambda = 1545.15$ nm, a maximum SFDR is obtained when $V_{REF} =$ -6 V. When we vary $V_G$ to -5.5 V and $V_{REF} =$ -3 V, a higher SFDR = 96dB/Hz$^{2/3}$ was obtained. The maximum achievable SFDR follows an envelope which is greatest at larger depletion biases $V_G$. Optical field scattering loss increases with stronger slow-light effect, resulting in reduced extinction ratio of the SLM in the slow light region. This additional loss factor contributes to a decrease in SFDR of a SLM at 1545.15nm.

### D. Slow-Light Effect on Modulator Slope Efficiency

The slope efficiency $s_m$ of a modulator is an important figure-of-merit which is defined as the derivative of the transfer function (T) at the bias point. For a MZM, it can be expressed as [26]

$$s_m = RP_L \frac{\partial T(\tilde{v}_m)}{\partial \tilde{v}_m}\bigg|_{V_{DC}} \approx -\frac{\pi T_{max} R P_L}{2V_\pi} \tag{5}$$

where $R$ is the modulator impedance and $P_L$ is optical input power. The subscript $m$ is used to denote which phase shifter

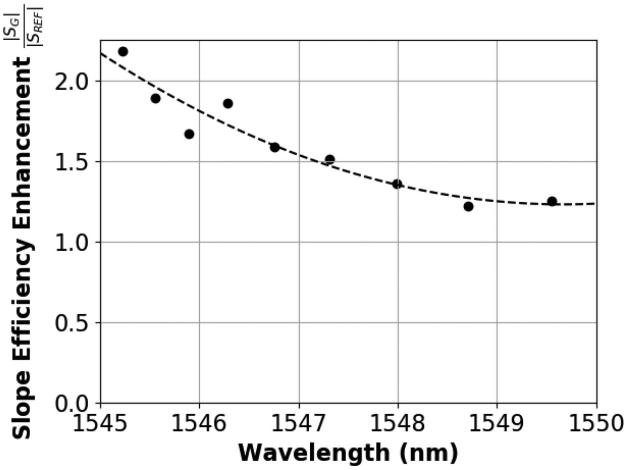


Fig. 7. SLM slope efficiency enhancement percentage versus wavelength in the slow-light region. Each datum is measured at a SLM quadrature point with $V_G = V_{REF} =$ -3 V. The dashed line is a fitting curve that serves as a guide to the eye.

the small signal $\tilde{v}_m$ will be applied to. $T_{max}$ is the peak of the SLM transfer function, corresponding to the maximum output power of the SLM that decreases near the band-edge due to increased scattering loss. The right-hand side of Eq. (5) gives an approximation of $s_m$ for an ideal sinusoidal transfer function, indicating that $s_m$ is generally proportional to $T_{max}$ and inversely proportional to $V_\pi$. Therefore, one simple approach to increase $s_m$ is to decrease $V_\pi$, generally by increasing the length L of the phase shifter arm. An increased L gives larger junction capacitance $C_m$, which in turn limits the bandwidth $f_{BW}$ of the modulator:

$$f_{BW} \propto \frac{1}{C_m}. \tag{6}$$

The link gain G is proportional to the square of slope efficiency [26]. Besides higher bandwidth, a smaller $V_\pi$ is also in favor of a better link gain:

$$G \propto s_m^2 \propto \frac{1}{V_\pi^2}. \tag{7}$$

The SLM has an increased modulation efficiency, $V_\pi \cdot L = \sim$1 V·cm due to enhanced optical field and plasma interaction, so a reduced $V_\pi$ of the SLM will also give rise to higher RF linear modulator slope efficiency. A slope efficiency enhancement (*SEE*) factor can be quantitatively evaluated by applying $\tilde{V}_{RF}$ to the grating arm in comparison with applying $\tilde{V}_{RF}$ to the reference arm under the same bias point and operating wavelength. The SEE is then defined as the relative change in slope efficiency expressed as a percentage:

$$SEE = \frac{|s_G| - |s_{REF}|}{|s_{REF}|} \times 100\%. \tag{8}$$

The measured SEE factor at selected quadrature points is depicted in Fig. 7, when $V_G = V_{REF} =$ -3 V. When operating near the band edge, the slow-light grating phase shifter demonstrate a SEE of 2.18 at $\lambda = 1545.15$ nm; and SEE decreases monotonically with wavelength as the slow-light effect weakens.

Overall, the slow-light grating phase shifter displayed the slow light effect in a range up to $\sim$ 4 nm from the band-edge. A residual SEE $= \sim$ 1.2 at $\lambda = 1550$ nm was observed, which could be caused by slight fabrication offsets of the junctions in each respective arm. The SLM demonstrates a solution to reduce $V_\pi$ without augmenting the phase shifter length which would otherwise increase the junction capacitance.

Though a Bragg grating is a dispersive optical element, the modulated RF signals are not further distorted by this dispersion, as they propagate through the grating phase shifter as a purely phase-modulated signal at the optical carrier frequency. It is only at the combiner of the MZI that the phase modulation leads to amplitude modulation, and the RF signals appear as optical sidebands which will propagate through the remainder of the RF link with unequal dispersion.

As pointed out earlier, the traveling wave electrode design of the SLM phase impact the bandwidth of the modulator. It is even more challenging to match the RF wave traveling speed to with the optical field with varying group velocity. In the future work, we will further reduce the SLM to $\sim$ 500 $\mu$m so that the phase shifter can be treated as a lumped device, eliminating the need of traveling RF electrodes.

## V. Conclusion

In this work, for the first time, a slow-light enhanced scheme for an integrated photonic silicon modulator. In contrast to typical dual-drive methods and conventional single-drive schemes, the DC bias across the reference arm and the operating wavelength can be controlled to maximize the small-signal linearity. Simultaneously, this control of the biases removes the need for external waveguide heaters to set the MZM at its quadrature point, giving rise to small device/system footprint and a simplified operation scheme. An enhanced modulation efficiency, $V_\pi.L_\pi = \sim$1 V·cm and a reduced $V_\pi$ is demonstrated in the slow-light region compared to those operating far from the grating band-edge. In the slow-light region, under moderate to large depletion conditions, the SLM is tested to have a SFDR of 96 dB/Hz$^{2/3}$. This work demonstrated the feasibility of a chip-scale RF link that consists of a SLM and integrated SiGe photodetector using foundry processing for RF photonic applications.

## Acknowledgment

S. R. Anderson thanks W. Zhou, S. Cho and E. Martin for the helpful discussions. He would also like to acknowledge the support of the DoD SMART Scholarship Program.

## References

[1] A. Rao et al., "Heterogeneous microring and Mach-Zehnder modulators based on lithium niobate and chalcogenide glasses on silicon," *Opt. Exp.*, vol. 23, no. 17, pp. 22746–22752, 2015.

[2] P. Rabiei, J. Ma, S. Khan, J. Chiles, and S. Fathpour, "Heterogeneous lithium niobate photonics on silicon substrates," *Opt. Exp.*, vol. 21, no. 21, pp. 25573–25581, 2013.

[3] P. De Dobbelaere, "Silicon photonics technology platform for embedded and integrated optical interconnect systems," in *Proc. 18th Asia South Pacific Des. Automat. Conf.*, 2013, pp. 644–647, doi: 10.1109/ASPDAC.2013.6509671.

[4] D. Patel, A. Samani, V. Veerasubramanian, S. Ghosh, and D. V. Plant, "Silicon photonic segmented modulator-based electro-optic DAC for 100gb/s PAM-4 generation," *IEEE Photon. Technol. Lett.*, vol. 27, no. 23, pp. 2433–2436, Dec. 2015.

[5] A. Khilo, C. M. Sorace, and F. X. Kärtner, "Broadband linearized silicon modulator," *Opt. Exp.*, vol. 19, no. 5, pp. 4485–4500, 2011.

[6] A. Gutierrez et al., "High linear ring-assisted MZI electro-optic silicon modulators suitable for radio-over-fiber applications," in *Proc. 9th Int. Conf. Group IV Photon.*, 2012, pp. 57–59.

[7] C. G. Bottenfield, V. A. Thomas, and S. E. Ralph, "Silicon photonic modulator linearity and optimization for microwave photonic links," *IEEE J. Sel. Top. Quantum Electron.,* vol. 25, no. 5, Sep./Oct. 2019, Art. no. 3400110.

[8] N. Hosseinzadeh, A. Jain, R. Helkey, and J. F. Buckwalter, "RF silicon photonics for wideband, high dynamic range microwave and millimeter-wave signal processing," in *Proc. IEEE 18th Topical Meeting Silicon Monolithic Integr. Circuits RF Syst.*, 2018, pp. 41–44, doi: 10.1109/SIRF.2018.8304224.

[9] M. Jacques, A. Samani, E. El-Fiky, D. Patel, Z. Xing, and D. V. Plant, "Optimization of thermo-optic phase-shifter design and mitigation of thermal crosstalk on the SOI platform," *Opt. Exp.*, vol. 27, no. 8, pp. 10456–10471, 2019.

[10] A. Melikyan, N. Kaneda, K. Kim, Y. Baeyens, and P. Dong, "Differential drive I/Qmodulator based on silicon photonic electro-absorption modulators," *J. Lightw. Technol.*, vol. 38, no. 11, pp. 2872–2876, Jun. 2020.

[11] M. Streshinsky et al., "Highly linear silicon traveling wave Mach–Zehnder carrier depletion modulator based on differential drive," *Opt. Exp.*, vol. 21, no. 3, pp. 3818–3825, 2013.

[12] G. Cong, M. Ohno, Y. Maegami, M. Okano, and K. Yamada, "Silicon traveling-wave Mach–Zehnder modulator under distributed-bias driving," *Opt. Lett.*, vol. 43, no. 3, pp. 403–406, 2018.

[13] N. Margalit, C. Xiang, S.M. Bowers, A. Bjorlin, R. Blum, and J.E. Bowers, "Perspective on the future of silicon photonics and electronics," *Appl. Phys. Lett.*, vol. 118, no. 22, 2021, Art. no. 220501.

[14] P. A. Morton, J. Cardenas, M. Lipson, and J. B. Khurgin, "Miniature, linearized silicon photonics modulators for phased array systems," in *Proc. IEEE Int. Topical Meeting Microw. Photon.*, 2013, pp. 275–277.

[15] S. Anderson, A. Begović, A. Chen, Z. R. Huang, W. Zhou, and G. Sun, "Integrated silicon photonic true-time delay beam-former for wide-band phased-array antenna," in *Proc. IEEE 70th Electron. Compon. Technol. Conf.*, 2020, pp. 162–167.

[16] Y. Hinakura, Y. Terada, H. Arai, and T. Baba, "Electro-optic phase matching in a Si photonic crystal slow light modulator using meander-line electrodes," *Opt. Exp.*, vol. 26, no. 9, pp. 11538–11545, 2018.

[17] Y. Hinakura, H. Arai, and T. Baba, "64 Gbps Si photonic crystal slow light modulator by electro-optic phase matching," *Opt. Exp.*, vol. 27, no. 10, pp. 14321–14327, 2019.

[18] A. Brimont et al., "High speed silicon electro-optical modulators enhanced via slow light propagation," *Opt. Exp.*, vol. 19, no. 21, pp. 20876–20885, 2011.

[19] L. Chrostowski and M. Hochberg, *Silicon Photonics Design: From Devices to Systems*. Cambridge, U.K.: Cambridge Univ. Press, 2015.

[20] L. Jiang and Z. R. Huang, "Integrated cascaded Bragg gratings for on-chip optical delay lines," *IEEE Photon. Technol. Lett.*, vol. 30, no. 5, pp. 499–502, Mar. 2018.

[21] R. Soref and B. Bennett, "Electrooptical effects in silicon," *IEEE J. Quantum Electron.*, vol. 23, no. 1, pp. 123–129, Jan. 1987.

[22] J. Cardenas et al., "Linearized silicon modulator based on a ring assisted Mach Zehnder inteferometer," *Opt. Exp.*, vol. 21, no. 19, pp. 22549–22557, 2013.

[23] S. Khan and S. Fathpour, "Demonstration of tunable optical delay lines based on apodized grating waveguides," *Opt. Exp.*, vol. 21, no. 17, pp. 19538–19543, 2013.

[24] Y. A. Vlasov and S. J. McNab, "Coupling into the slow light mode in slab-type photonic crystal waveguides," *Opt. Lett.*, vol. 31, no. 1, pp. 50–52, 2006.

[25] F. Y. Gardes, G. T. Reed, C.E., Png, and N. G. Emerson, "A sun-micro depletion-type photonic modulator in silicon on insulator," *Opt. Exp.*, vol. 13, no. 22, pp. 8845–8854, Oct. 2005.

[26] W. S. Chang, *RF Photonic Technology in Optical Fiber Links*. Cambridge, U.K.: Cambridge Univ. Press, 2002.

[27] X. Luo et al., "Slope efficiency and spurious-free dynamic range of silicon Mach–Zehnder modulator upon carrier depletion and injection effects," *Opt. Exp.*, vol. 21, no. 14, pp. 16570–16577, 2013.